Distinct brain iron profiles associated with logopenic progressive aphasia and posterior cortical atrophy

Neha Atulkumar Singh [a], Arvin Arani [b], Jonathan Graff-Radford [a], Matthew L. Senjem [b], Peter R. Martin [c], Mary M. Machulda [d], Christopher G. Schwarz [b], Yunhong Shu [b], Petrice M. Cogswell [b], David S. Knopman [a], Ronald C. Petersen [a], Val J. Lowe [b], Clifford R. Jack Jr. [b], Keith A. Josephs [a], Jennifer L. Whitwell [b,*]

[a] Department of Neurology, Mayo Clinic, Rochester, MN, USA
[b] Department of Radiology, Mayo Clinic, Rochester, MN, USA
[c] Department of Quantitative Health Sciences, Mayo Clinic, Rochester, MN, USA
[d] Department of Psychiatry & Psychology, Mayo Clinic, Rochester, MN, USA

ARTICLE INFO

ABSTRACT

Quantitative susceptibility mapping (QSM) can detect iron distribution in the brain by estimating local tissue magnetic susceptibility properties at every voxel. Iron deposition patterns are well studied in typical Alzheimer's disease (tAD), but little is known about these patterns in atypical clinical presentations of AD such as logopenic progressive aphasia (LPA) and posterior cortical atrophy (PCA). Seventeen PCA patients and eight LPA patients were recruited by the Neurodegenerative Research Group at Mayo Clinic, Rochester, MN, and underwent MRI that included a five-echo gradient echo sequence for calculation of QSM. Mean QSM signal was extracted from gray and white matter for regions-of-interest across the brain using the Mayo Clinic Adult Lifespan Template. Bayesian hierarchical models were fit per-region and per-hemisphere to compare PCA, LPA, 63 healthy controls, and 20 tAD patients. Strong evidence (posterior probability > 0.99) was observed for greater susceptibility in the middle occipital gyrus and amygdala in both LPA and PCA, and in the right inferior parietal, inferior temporal, and angular gyri in PCA and the caudate and substantia nigra in LPA compared to controls. Moderate evidence for greater susceptibility (posterior probability > 0.90) was also observed in the inferior occipital gyrus, precuneus, putamen and entorhinal cortex in both LPA and PCA, along with superior frontal gyrus in PCA and inferior temporal gyri, insula and basal ganglia in LPA, when compared to controls. Between phenotypic comparisons, LPA had greater susceptibility in the caudate, hippocampus, and posterior cingulate compared to PCA, while PCA showed greater susceptibility in the right superior frontal and middle temporal gyri compared to LPA. Both LPA and PCA showed moderate and strong evidence for greater susceptibility than tAD, particularly in medial and lateral parietal regions, while tAD showed greater susceptibility in the hippocampus and basal ganglia. This study proposes the possibility of unique iron profiles existing between LPA and PCA within cortical and subcortical structures. These changes match well with the disease-related changes of the clinical phenotypes, suggesting that QSM could be an informative candidate marker to study iron deposition in these patients.

1. Introduction

Dysregulation of iron metabolism has been proposed to play an important role in typical Alzheimer's disease (tAD) (Lane, Ayton, and Bush 2018) with multiple studies associating the presence of brain iron with either clinical deterioration of tAD (Ayton et al. 2020), or its pathology: beta amyloid (Aβ) plaques (Telling et al. 2017) and neurofibrillary tangles (Yamamoto et al. 2002).

A recently proposed non-invasive magnetic resonance imaging (MRI) technique for measuring iron accumulation is quantitative susceptibility mapping (QSM), which can detect iron distribution in the brain by estimating local tissue magnetic susceptibility properties for every voxel (Wang and Liu 2015). Susceptibility sources can be classified into two major types: paramagnetic (positive magnetic susceptibility) and diamagnetic (negative magnetic susceptibility) (Liu et al. 2015). Some susceptibility sources in the human brain are cerebral iron (ferritin-strongly paramagnetic) (Liu et al. 2015), iron containing sources (mostly strongly paramagnetic): such as deoxyhemoglobin in veins (contains ferrous molecules) (Wang and Liu 2015) and neuromelanin (iron containing complex), along with myelin (weakly diamagnetic) (Liu et al. 2015).

Since the paramagnetic and diamagnetic sources are co-localized in the AD brain, one could theorize that they may generate a counteracting effect on the QSM values, but multiple studies on the subject lend evidence counter to such theories. Langkammer *et.al.,* studied the iron concentrations in post-mortem tissue and the bulk magnetic susceptibility in gray matter structures and found strong linear correlations between the two, suggesting that iron content contributed to the bulk of the QSM signal (Langkammer et al. 2012). Similarly, Tiepolt *et.al.,* examined the differences in susceptibility signatures in AD cases to better understand the counteracting effects of paramagnetic and diamagnetic sources, and reported that any counteracting effect of the two sources would have to be minimal (Tiepolt et al. 2020). Together, these studies support Hallgren *et.al.,* initial findings that the dominant source of magnetic susceptibility in the gray matter is iron (Hallgren and Sourander 1958) and can be assessed with QSM (Ravanfar et al. 2021), making QSM an informative marker to study brain iron deposition.

The distribution of iron in the brain has been studied in tAD using QSM. Multiple structures with high iron levels have been identified, including the basal ganglia, medial temporal gyrus, inferior deep gray nuclei (substantia nigra, red nucleus and subthalamic nucleus), sensorimotor strip and precuneus (Kim et al. 2017; Cogswell et al. 2021). However, little is known about the distribution of iron in the atypical clinical presentations of AD such as logopenic progressive aphasia (LPA) and posterior cortical atrophy (PCA), where LPA is characterized by language deficits, including poor word retrieval, difficulty repeating sentences and phonological errors (Gorno-Tempini et al. 2011; Botha et al. 2015) and PCA by visuospatial and visuoperceptual deficits (Tsai et al. 2011; Crutch et al. 2017).

Therefore, the goals of the current study were to i) describe the brain iron distribution patterns within cortical and subcortical regions in PCA and LPA compared to healthy controls, ii) evaluate if QSM patterns of iron deposition could differentiate between PCA and LPA, iii) assess if these patterns differed between the atypical and typical variants of AD. Given that LPA and PCA show different patterns of brain neurodegeneration, we hypothesized that they would show different regional patterns of iron deposition, and that these regional patterns would differ from tAD.

2. Methods

2.1. Patients

Seventeen patients who met clinical diagnostic criteria for PCA (Crutch et al. 2017) and eight patients who met imaging-supported clinical diagnostic criteria for LPA (Gorno-Tempini et al. 2011; Botha et al. 2015) were recruited by the Neurodegenerative Research group (NRG) at Mayo Clinic, Rochester, MN, between October 01, 2020 and May 23, 2022. All patients were enrolled into the study regardless of age and underwent extensive neurological evaluations performed by one of two behavioral neurologists (KAJ or JGR) and neuropsychological testing overseen by a neuropsychologist (MMM). All clinical diagnoses were rendered by consensus between both behavioral neurologists after review of clinical history and results of clinical testing. All patients underwent an MRI protocol that included a five-echo gradient echo sequence for calculation of QSM. A cohort of 63 cognitively normal healthy individuals were recruited by the NRG between November 11, 2020 and April 21, 2022 and underwent identical MRI scans. All three cohorts were age-matched to avoid any confounding effect of age. Furthermore, a cohort of 20 patients who met the clinical criteria for tAD (McKhann et al. 2011) who were recruited by the Mayo Clinic Alzheimer's Disease Research Center (ADRC) and had undergone identical MRI scans were identified. These 20 tAD patients were selected to be representative of late-onset tAD and hence were not age-matched with the other cohorts.

2.2. Patient consent and protocols

The study was approved by the Mayo Clinic IRB. All patients gave written informed consent to participate in this study.

2.3. Clinical testing

The neurological evaluations performed on the PCA and LPA patients included the Montreal Cognitive Assessment Battery (MoCA) for assessing general cognitive function (Nasreddine et al. 2005). Language assessments included the Boston Naming Test (BNT) for assessing confrontational naming (Lansing et al. 1999), and the Boston Diagnostic Aphasia Examination (BDAE) repetition subtest for assessing sentence repetition (Goodglass and Barresi 2000). The Sydney language battery semantic association subtest was administered to the LPA patients to ensure sparing of object knowledge (Savage et al. 2013) and the Pyramids and Palm Trees word-word matching test was administered to ensure sparing of word knowledge (Howard and Patterson 1992). Motor speech was assessed during spontaneous speech and was spared in all patients. The battery also included the Rey-Osterrieth Complex Figure Test (Rey-O) to assess visuospatial constructional ability (Osterrieth 1944), the Visual Object and Space Perception Battery (VOSP) Cubes test for assessing visuospatial ability and Letters test for assessing visuoperceptual ability (Warrington and James 1991), and the Western Aphasia Battery ideomotor apraxia subtest to assess ideomotor praxis (Kertesz 2007). Specific characteristics of PCA were also documented, including the presence/absence of features of Balint's syndrome, Gerstmann's syndrome, visual field defect, apperceptive prosopagnosia and dressing apraxia. A subject was considered to have features of Balint's syndrome if they had any one of the following symptoms: oculomotor apraxia, optic ataxia, and simultanagnosia. Oculomotor apraxia and optic ataxia were assessed on neurological examination. The severity of simultanagnosia was determined on a 20-point scale with 20 being the best score. The simultanagnosia test was designed to assess the individuals ability to perceive the overall meaning/shape of the figure/object/picture instead of recognizing bits and pieces, and included, for example, pictures of overlapping line drawings, pictures of fragmented numbers, and pictures of objects/letters whose shape was created from smaller items (Tetzloff et al. 2018). Apperceptive prosopagnosia was assessed by asking the subject to select the one famous face from a panel of three similar looking faces, for a total of 10 different panels. A patient was considered to have features of Gerstmann's syndrome if they had any one of following symptoms: acalculia (3 or less on MoCA calculation), left–right confusion, agraphia, or finger agnosia. In addition, the Rey Auditory Verbal Learning Test – Recognition Percent Correct (AVLT-RCP) was used to assess episodic memory. The neurological

evaluations performed on the tAD patients from the ADRC included the MoCA.

2.4. Image acquisition

All patients underwent a standardized MRI protocol on one 3 T Siemens Prisma scanner at Mayo Clinic, Rochester, MN. The protocol included a T1-weighted magnetization prepared rapid gradient echo (MPRAGE) sequence (TR/TE/T1 = 2300/3.14/945 ms; flip angle 9°, 0.8 isotropic resolution). For QSM acquisition, a 3D multi-echo GRE (3D-MEGRE) acquisition consisting of five echoes with acquisition parameters: TR 28 ms; TE 6.7, 10.6, 14.5. 18.4 and 22.5 ms, flip angle 15°, field of view (FOV) 200 mm, acquired matrix 384 × 269, reconstructed in-plane resolution 0.52 mm^2, slice thickness 1.8 mm, slices, 88, GRAPPA Ry = 2, acquisition time 6 mins 37 secs were used to process the 3D-MEGRE data and generate QSM maps using a publically available software package (STI suite, https://www.eecs.berkeley.edu/~chunlei.liu /software.html) (Cogswell et al. 2021).

2.5. Image processing

First the affine registration parameters were computed between the T1-weighted images and mean of the magnitude GRE images across the echo times. Laplacian-based phase unwrapping was applied, and the masking was performed based on the T1-weighted segmentation. Sparse linear equations and least squares method was applied to compute the QSM from the unwrapped, masked phase data (Li, Wu, and Liu 2011). Detailed acquisition details have been previously published (Cogswell et al. 2021). Mean QSM signal was extracted from gray and white matter for twenty-six regions-of-interest (ROIs), along with their corresponding right and left ROIs, across the brain using the Mayo Clinic Adult Lifespan Template (MCALT) atlas (MCALT: https://www.nitrc.org/projects/mcalt/).

Twenty-six ROIs were assessed: superior frontal gyrus, superior temporal, middle temporal, inferior temporal, amygdala, hippocampus, entorhinal cortex, insula, posterior cingulum, precuneus, retrosplenial cortex, superior parietal, inferior parietal, angular gyrus, supramarginal gyrus, superior occipital, middle occipital, inferior occipital and subcortical structures: caudate, putamen, pallidum, thalamus, subthalamic nucleus, red nucleus, substantia nigra, cerebellar dentate.

2.6. Statistical analysis

To generate profiles of susceptibility for PCA and LPA as well as compare regional susceptibility in PCA and LPA to susceptibility in healthy controls and tAD, region-and-hemisphere specific bayesian hierarchical linear models predicting susceptibility as the outcome by diagnosis group as the predictor were used. The first model compared PCA and LPA to controls and to each other, and the second model compared PCA and LPA to tAD. Each of these models yielded an intercept per diagnosis group, which allowed us to compare cross-sectional susceptibility within region and hemisphere across diagnoses. More specifically, these intercepts were estimated as random effects, thereby pooling information within region-and-hemisphere and shrinking estimates toward an overall median susceptibility within region, which resulted in shrunken estimates that are more generalizable and prospectively managing the problem of multiple comparisons (Greenland 2000; Gelman and Hill (2007)). Shrinkage estimators introduce helpful bias toward the null, reducing the influence of outliers. Partial pooling of variances also reduces the impact of a single patient unduly influencing results; if a patient is high across multiple regions, the random effect for that patient will incorporate that global information, decreasing the effect of that patient across all regions. The multi-region models are thus protected from the inflated type I error that would be associated with many single-region models, the problem of multiple comparisons, while also increasing statistical power to detect true effects.

These models were fit using the statistical software R (R Core, Team (2020)) in conjunction with the rstanarm package (Goodrich et al. 2020) version 2.21.1 running STAN version 2.21.0 (Stan Development, Team (2017)). Each model used eight chains of 4000 samples, with the first half of samples discarded as burn in, resulting in posterior samples of 16,000 estimates per parameter. The effective sample size for each of these parameters was at least in the multiple thousands and the $\hat{R}$ (R "hat"), a measure of posterior convergence, was approximately-one for all parameters across all models, indicating no lack of fit in any of these models.

These posterior samples provided distributions for each model parameter, and we then summarize these distributions using probabilities. We assessed the proportion of the distribution that was greater than zero and compared the proportion of samples from one estimate that was greater than a second estimate (comparing PCA and LPA intercepts, for example). The results of these comparisons were reported as posterior probabilities, denoted as Pb in this paper, and we considered Pb > 0.90 or < 0.10 as moderate evidence of a difference and Pb > 0.99 or < 0.01 as strong evidence of a difference. We have these upper and lower bounds because in the Bayesian paradigm we are not biased using one-sided tests (indeed we can only set up one-sided comparisons using these posterior probabilities), and it is simple to show that if there is 0.08 probability that X > Y, then we can also say that the probability Y > X is 0.92.

3. Results

3.1. Study demographics

The demographic and clinical features of the cohorts are shown in Table 1. The PCA and LPA groups did not differ on sex, education, age, or disease duration at MRI. On clinical testing, the PCA group performed worse than the LPA group on Rey-O complex figure (p < 0.001), VOSP cubes (p = 0.001), and VOSP letters (p=<0.001).

3.2. Regional susceptibility in PCA and LPA compared to healthy controls

Example QSM images from a healthy control, tAD and a PCA and LPA patient are shown in Fig. 1. High susceptibility was observed in the basal ganglia and deep gray matter nuclei (substantia nigra, red nucleus and subthalamic nucleus) in all four cases.

The results of the bayesian hierarchical linear model comparing PCA, LPA and controls are shown in Fig. 2 and Table 2. In PCA, there was strong evidence of greater susceptibility in the middle occipital gyrus, inferior parietal, angular and inferior temporal gyri, along with amygdala when compared to healthy controls. There were also regions that showed moderate evidence of difference compared to controls with greater susceptibility in the inferior occipital gyrus, precuneus, right superior frontal gyrus and entorhinal cortex, with lower susceptibility in the left superior parietal and supramarginal gyri, along with hippocampus.

In LPA, there was strong evidence of greater susceptibility in the left middle occipital gyrus and amygdala, compared to healthy controls. Moderate evidence of difference compared to controls was seen with greater susceptibility in the left inferior temporal gyrus, superior parietal and inferior parietal gyrus, and angular gyrus, left precuneus and inferior occipital gyrus, insula, caudate, putamen, substantia nigra and entorhinal cortex, with lower susceptibility in the right superior temporal and middle temporal gyri.

When comparing PCA and LPA, LPA showed strong evidence of greater susceptibility in the caudate and moderate evidence of greater susceptibility in the hippocampus and posterior cingulum compared to PCA, while PCA showed moderate evidence of greater susceptibility in the right superior frontal and middle temporal gyri with retrosplenial cortex compared to LPA.

Table 1
Participant's demographics and disease characteristics.

	Disease cohort (N = 19)			Disease controls			Healthy controls		
	PCA (N = 17)	LPA (N = 8)	P-value	tAD (N = 20)	vs PCA P-value	vs LPA P-value	(N = 63)	vs PCA P-value	vs LPA P-value
Female, n (%)	14 (82 %)	5 (62 %)	0.344	14 (70 %)	0.462	> 0.999	46 (73 %)	0.540	0.678
Education, yr	16 (12, 18)	16 (15, 16)	0.835	16 (14, 17)	0.744	0.833	16 (15, 18)	0.341	0.435
Age at onset, yr	56 (52, 59)	60 (58, 67)	0.268	76 (72, 79)	< 0.001	0.001	–	–	–
Age at scan, yr	63 (58, 64)	65 (62, 72)	0.180	80 (77, 82)	< 0.001	< 0.001	65 (59, 69)	0.140	0.513
Disease duration, yr	4.4 (3.1, 6.0)	4.8 (3.5, 6.0)	0.600	2.4 (0.7, 5.3)	0.143	0.114	–	–	–
MoCA (30)	17 (12, 19)	7 (6, 14)	0.171	16 (13, 20)	0.605	0.048	27 (26, 28)	< 0.001	< 0.001
BNT (15)	11 (6, 12)	8 (5, 10)	0.256	–	–	–	–	–	–
BDAE repetition (10)	8 (6, 9)	4 (3, 8)	0.101	–	–	–	–	–	–
SYDBAT semantic association (/0)	–	26 (22, 27)	–	–	–	–	–	–	–
PPT word-word (52)	50 (48, 50)	49 (47, 50)	0.259						
Rey-O MOANS	2 (2, 2)	6 (4, 8)	< 0.001	–	–	–	–	–	–
VOSP cubes (10)	0 (0, 1)	10 (3, 10)	0.001	–	–	–	–	–	–
VOSP letter (20)	6 (0, 8)	20 (18, 20)	< 0.001	–	–	–	–	–	–
Simultanagnosia (20)	5 (2, 7)	18 (16, 19)	< 0.001						
AVLT RCP (1 0 0)	80 (67, 90)	63 (55, 72)	0.139	–	–	–	–	–	–
WAB praxis subscore (/60)	59 (55, 60)	58 (55, 60)	0.793	–	–	–	–	–	–
Feature of Balint's syndrome, n (%)	17 (100 %)	2 (25 %)	–	–	–	–	–	–	–
Features of Gerstmann syndrome, n (%)	16 (94 %)	0 (0 %)	–	–	–	–	–	–	–
Visual field defect, n (%)	10 (59 %)	0 (0 %)	–	–	–	–	–	–	–
Apperceptive prosopagnosia, n (%)	4 (24 %)	0 (0 %)	–	–	–	–	–	–	–
Dressing apraxia, n (%)	7 (41 %)	0 (0 %)	–	–	–	–	–	–	–

Data shown are n (%) or median (first and third quartiles). For continuous variables, p-values are from Wilcoxon Rank Sum test. For categorical variables, p-values are from Fisher's Exact test. Key; PCA, Posterior Cortical Atrophy; LPA, Logopenic Progressive Aphasia; HC, Healthy controls; tAD, typical Alzheimer's Disease; MoCA, Montreal Cognitive Assessment Battery; BNT, Boston Naming Test; BDAE, Boston Diagnostic Aphasia Exam; MOANS, Mayo older adult norms, Rey-O, Rey-Osterrieth Complex Figure Test; VOSP, Visual Object and Space Perception Battery; AVLT-RCP, Auditory Verbal Learning Test – Recognition Percent Correct; SYDBAT, Sydney Language Battery; WAB, Western Aphasia Battery; PPT, Pyramid and Palm Trees. MOANS scores are age corrected and constructed to have a mean of 10 and standard deviation of 3 among cognitively healthy subjects.
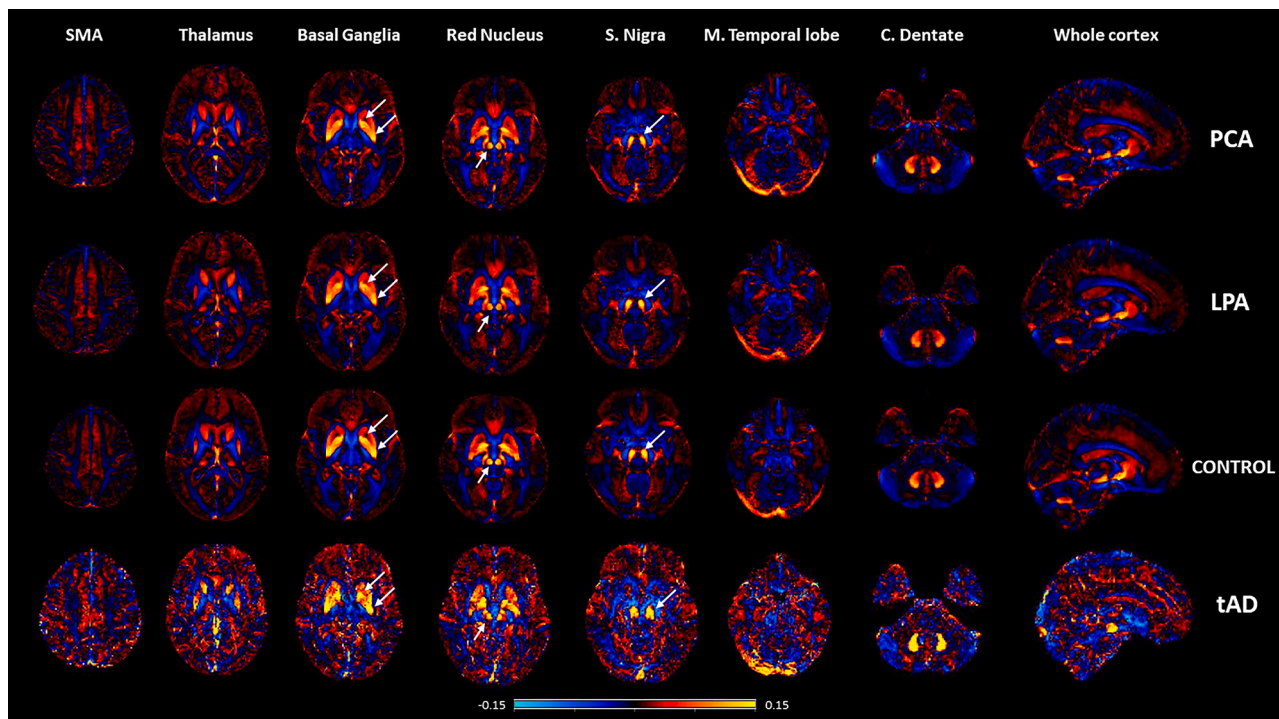

Fig. 1. QSM images from representative patients. Multiple slices of QSM images from a healthy control, tAD, a PCA and LPA patient are shown here. The paramagnetic values on the QSM are indicated in red to yellow, while the diamagnetic values are shown in blue. Regions with high iron deposition (paramagnetic susceptibility) are indicated in white arrows.

3.3. Regional susceptibility in PCA and LPA compared to tAD

The results of the bayesian hierarchical linear model comparing PCA and LPA to tAD are shown in Fig. 3 and Table 3. There was strong evidence of greater susceptibility in the precuneus, inferior temporal gyrus and insula in PCA compared to tAD, and moderate evidence of greater susceptibility in the inferior occipital, middle temporal, superior frontal, and angular gyri, with the amygdala and entorhinal cortex.
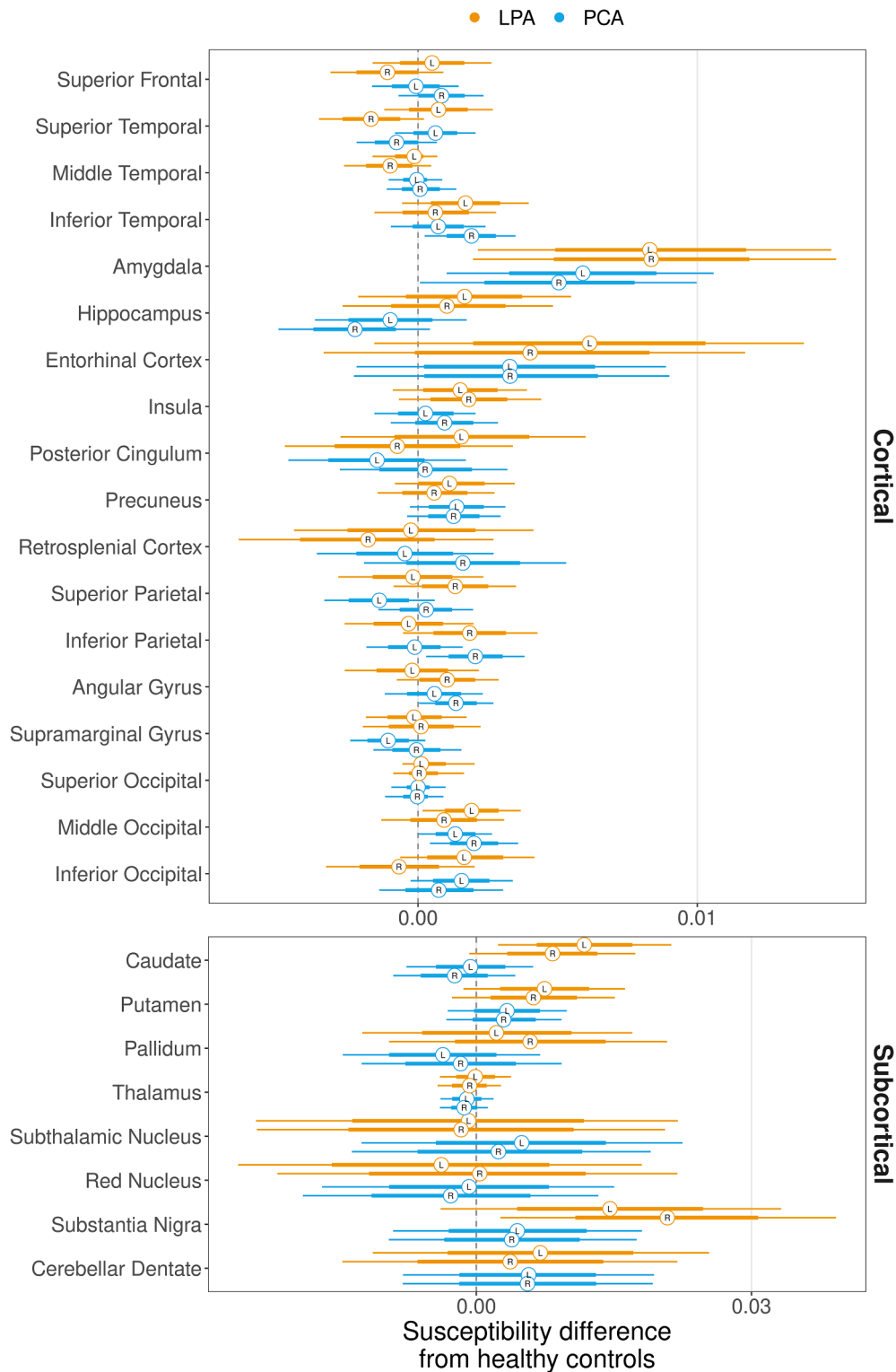
Fig. 2. Forest plots comparing PCA and LPA to healthy controls. The plot shows estimates (median), 80 % posterior interval (thick line) and 98 % posterior interval (thin line). It is interpreted as follows; when the 80 % posterior interval does not touch zero, we say there is moderate evidence (Pb > 0.90) of difference and when the 98 % posterior interval does not touch zero, we say there is strong evidence (Pb > 0.99) of difference from healthy controls.

Conversely, tAD only showed moderate evidence of difference with greater susceptibility in the hippocampus, caudate, pallidum and putamen compared to PCA.

LPA showed strong evidence of greater susceptibility in the insula and amygdala compared to tAD, and moderate evidence of difference with greater susceptibility in the precuneus, middle occipital gyrus, entorhinal cortex and caudate. Conversely, tAD only showed moderate evidence of greater susceptibility in the retrosplenial cortex and pallidum compared to LPA.

Table 2
Posterior probabilities of susceptibility differences between PCA, LPA and Healthy controls.

	Region	PCA > LPA		PCA > Healthy Controls		LPA > Healthy Controls	
		Left	Right	Left	Right	Left	Right
Corticals	Superior Frontal	0.284	0.975	0.458	0.905	0.709	0.103
	Superior Temporal	0.449	0.841	0.844	0.104	0.814	0.019
	Middle Temporal	0.614	0.928	0.407	0.558	0.294	0.053
	Inferior Temporal	0.186	0.885	0.842	0.997	0.961	0.749
	Amygdala	0.218	0.139	0.997	0.991	0.999	0.998
	Hippocampus	0.078	0.033	0.197	0.026	0.844	0.745
	Entorhinal Cortex	0.220	0.416	0.915	0.914	0.970	0.894
	Insula	0.145	0.239	0.637	0.877	0.929	0.955
	Posterior Cingulum	0.074	0.688	0.137	0.581	0.796	0.338
	Precuneus	0.601	0.759	0.968	0.964	0.901	0.742
	Retrosplenial Cortex	0.461	0.939	0.368	0.843	0.446	0.167
	Superior Parietal	0.172	0.159	0.050	0.649	0.438	0.925
	Inferior Parietal	0.582	0.570	0.430	0.997	0.360	0.963
	Angular Gyrus	0.756	0.633	0.780	0.991	0.413	0.912
	Supramarginal Gyrus	0.144	0.434	0.033	0.469	0.425	0.548
	Superior Occipital	0.320	0.368	0.506	0.438	0.701	0.594
	Middle Occipital	0.252	0.849	0.991	0.998	0.995	0.839
	Inferior Occipital	0.466	0.870	0.974	0.784	0.948	0.264
Subcorticals	Caudate	0.004	0.010	0.414	0.198	0.998	0.983
	Putamen	0.170	0.221	0.884	0.872	0.976	0.952
	Pallidum	0.205	0.150	0.213	0.359	0.638	0.821
	Thalamus	0.309	0.362	0.203	0.118	0.475	0.307
	Subthalamic Nucleus	0.692	0.654	0.754	0.638	0.467	0.428
	Red Nucleus	0.615	0.384	0.454	0.343	0.341	0.515
	Substantia Nigra	0.131	0.031	0.779	0.752	0.968	0.996
	Cerebellar dentate	0.440	0.581	0.832	0.831	0.814	0.683

The posterior probabilities of differences in susceptibility between diagnosis groups were calculated based on the region-specific Bayesian models. In this table, any values below 0.10 or above 0.90 indicate moderate evidence of a difference in susceptibility and are highlighted in light grey and values above 0.99 or below 0.01 indicate strong evidence of a difference in susceptibility between groups and are highlighted darker grey.

3.4. Effect of age on regional susceptibility in healthy controls

The results of the bayesian hierarchical linear model are shown in Fig. 4 and Table 4. There was strong evidence of lower susceptibility in the substantia nigra, red nucleus and cerebellar dentate, with moderate evidence in the subthalamic nucleus, with older age at scan.

4. Discussion

This study investigated regional patterns of iron deposition in PCA and LPA. We demonstrate that elevated QSM susceptibility is observed in both PCA and LPA, particularly in occipital, parietal, and lateral and medial temporal regions, and that regional differences are observed between PCA and LPA. Furthermore, PCA and LPA showed evidence for greater cortical susceptibility than tAD, even though the tAD cohort was older.

Susceptibility in PCA was elevated bilaterally in the occipital lobe, and in right parietal and temporal regions. These iron deposition patterns match well with the biological signature of the phenotype whereby neurodegeneration is observed in posterior regions of the brain (Josephs et al. 2006; Crutch et al. 2012; Whitwell et al. 2007), often with greater involvement of the right hemisphere (Whitwell et al. 2007; Lehmann et al. 2011). Elevated susceptibility was, however, also observed in some medial temporal structures. These structures are typically considered to be relatively spared in PCA compared to the striking involvement of the posterior cortex, although our group recently reported that mild to moderate medial temporal atrophy is common (Josephs et al. 2022). The precuneus and superior frontal gyrus also showed higher susceptibilities in PCA. This is in line with the literature as atrophy in the precuneus has recently been associated impairment of autobiographical memory in PCA (Ahmed et al. 2018), while atrophy in the superior frontal gyrus is commonly associated with visuospatial cognitive decline (Valdes Hernandez et al. 2018).

Elevated susceptibility in LPA was observed in similar regions, including the lateral temporal, occipital, parietal, and medial temporal lobes, with most findings stronger in the left hemisphere. LPA is a left-dominant phenotype which encompasses atrophy in lateral temporal and inferior parietal regions (Gorno-Tempini et al. 2004; Rohrer et al. 2013; Madhavan et al. 2013; Botha et al. 2015). The left-sided nature of the iron deposition, particularly in the inferior temporal gyrus with trends in the superior temporal gyrus, therefore, concurs with the typical patterns of asymmetric neurodegeneration (Lombardi et al. 2021). However, the regional distribution of iron deposition diverges somewhat from the expected pattern given the strong findings in the occipital lobe. The occipital cortices (Garcia-Azorin et al. 2014; Ramanan et al. 2020) and medial temporal regions (Rohrer et al. 2013) can become involved over time in LPA but are not usually the most atrophic regions early in the disease. We also noted moderate elevation in the amygdala and insula. While not the focus of neurodegeneration, these regions have been implicated in LPA. Studies have observed considerable reduction in the hippocampus/amygdala complex (Lombardi et al. 2021) and the insula (Lombardi et al. 2021; Ballard et al. 2014) volume in LPA at baseline, with significant reductions in the hippocampus/amygdala complex volume also noted at follow up, compared to controls in one study (Lombardi et al. 2021).

There were also regions where PCA and LPA showed lower susceptibility than controls, including in the supramarginal gyrus, hippocampus, and left superior parietal in PCA, and the right superior and middle temporal gyri in LPA. The reason for lower susceptibility in these regions is unclear, although it does highlight the pattern of relative sparing of certain regions based on diagnosis compared to controls, with the PCA showing sparing of the hippocampus, left superior parietal and supramarginal gyri and LPA for the right superior and middle temporal gyri. Multiple studies have reported elevated iron deposition in these regions in healthy individuals, suggesting that iron deposition may simply be a part of normal ageing, without the need of an existing or developing a disease. A similar effect, in the form of iron concentrations versus increasing age, has been seen in the basal ganglia and the inferior deep gray nuclei in healthy brains (Lin, Chao, and Wu 2015). Heathy ageing has also been associated with an increase in hippocampal iron levels
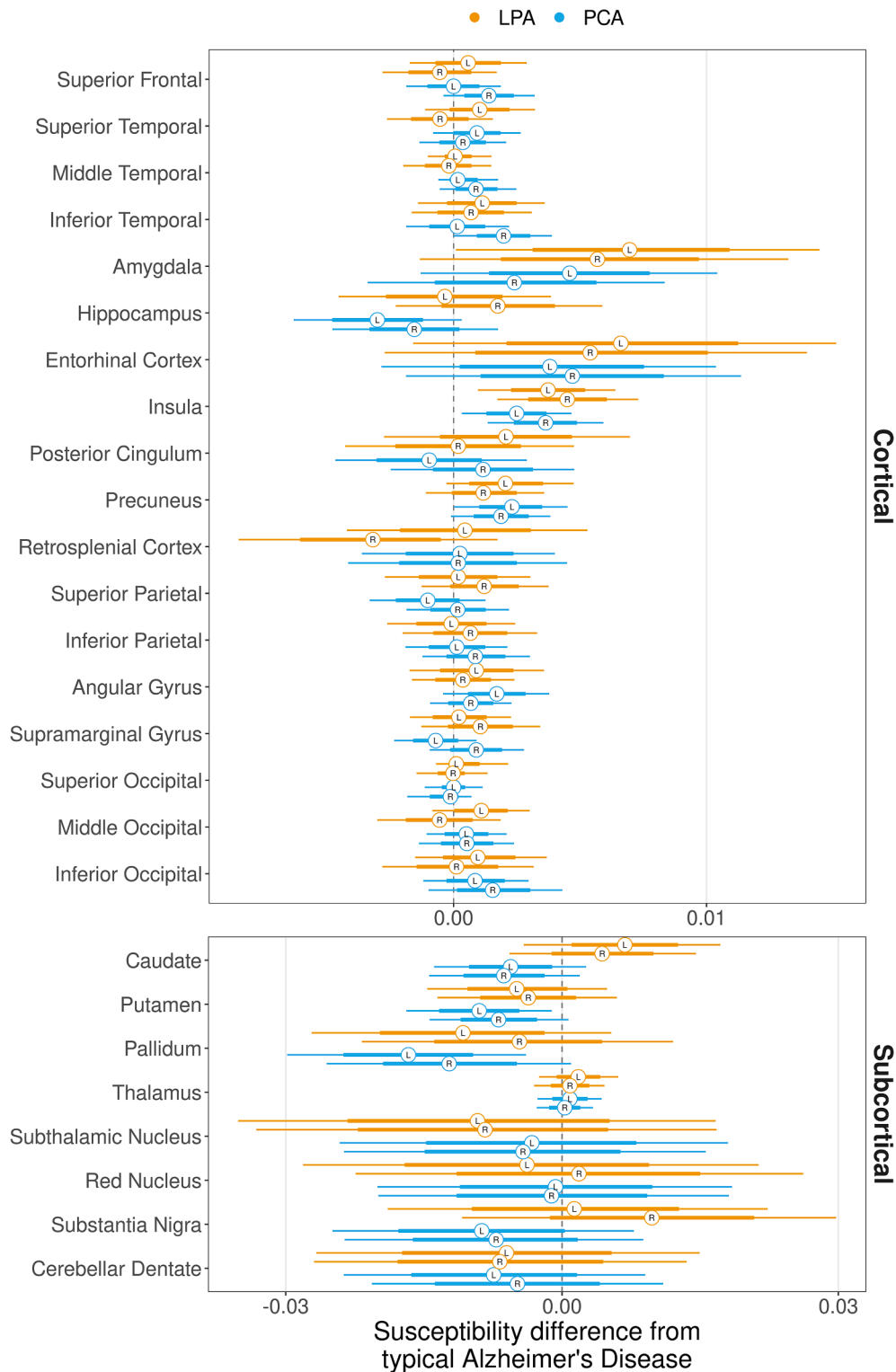
Fig. 3. Forest plots comparing PCA and LPA to tAD. The plot shows estimates (median), 80 % posterior interval (thick line) and 98 % posterior interval (thin line). It is interpreted as follows; when the 80 % posterior interval does not touch zero, we say there is moderate evidence (Pb > 0.90) of difference and when the 98 % posterior interval does not touch zero, we say there is strong evidence (Pb > 0.99) of difference from tAD.

(Bartzokis et al. 2011).

We observed regional differences between PCA and LPA, with PCA showing elevated susceptibility in the superior frontal and middle temporal gyri, and LPA showing elevated susceptibility in the left parietal lobe and subcortical regions (Tetzloff et al. 2018; Dronse et al. 2017). PCA and LPA also both showed greater susceptibility than tAD in

the insula and precuneus, with moderate susceptibility differences in some structures in the medial and lateral temporal lobes, inferior parietal, and inferior occipital gyri. These differences match well with the signatures of both atypical AD phenotypes and were observed even though the tAD group was approximately a decade older (Josephs et al. 2006; Rohrer et al. 2013; Josephs et al. 2022). Conversely, tAD showed

Table 3
Posterior probabilities of susceptibility differences between PCA, LPA and tAD.

	Region	PCA > LPA		PCA > tAD		LPA > tAD	
		Left	Right	Left	Right	Left	Right
Corticals	Superior Frontal	0.284	0.975	0.500	0.967	0.717	0.293
	Superior Temporal	0.449	0.841	0.898	0.698	0.869	0.269
	Middle Temporal	0.614	0.928	0.723	0.920	0.615	0.395
	Inferior Temporal	0.186	0.885	0.569	0.990	0.850	0.749
	Amygdala	0.218	0.139	0.965	0.834	0.991	0.970
	Hippocampus	0.078	0.033	0.016	0.132	0.421	0.845
	Entorhinal Cortex	0.220	0.416	0.913	0.951	0.971	0.937
	Insula	0.145	0.239	0.997	1.000	0.999	1.000
	Posterior Cingulum	0.074	0.688	0.280	0.775	0.846	0.538
	Precuneus	0.601	0.759	0.991	0.987	0.974	0.889
	Retrosplenial Cortex	0.461	0.939	0.561	0.542	0.591	0.064
	Superior Parietal	0.172	0.159	0.151	0.576	0.560	0.877
	Inferior Parietal	0.582	0.570	0.557	0.832	0.467	0.724
	Angular Gyrus	0.756	0.633	0.970	0.836	0.792	0.669
	Supramarginal Gyrus	0.144	0.434	0.154	0.869	0.602	0.854
	Superior Occipital	0.320	0.368	0.499	0.302	0.682	0.445
	Middle Occipital	0.252	0.849	0.776	0.740	0.904	0.297
	Inferior Occipital	0.466	0.870	0.830	0.922	0.807	0.539
Subcorticals	Caudate	0.004	0.010	0.058	0.033	0.935	0.847
	Putamen	0.170	0.221	0.004	0.017	0.126	0.181
	Pallidum	0.205	0.150	0.001	0.016	0.061	0.253
	Thalamus	0.309	0.362	0.710	0.587	0.836	0.709
	Subthalamic Nucleus	0.692	0.654	0.356	0.303	0.210	0.209
	Red Nucleus	0.615	0.384	0.464	0.441	0.361	0.573
	Substantia Nigra	0.131	0.031	0.108	0.150	0.561	0.869
	Cerebellar dentate	0.440	0.581	0.150	0.242	0.247	0.217

The posterior probabilities of differences in susceptibility between diagnosis groups were calculated based on the region-specific Bayesian models. In this table, any values below 0.10 or above 0.90 indicate moderate evidence of a difference in susceptibility and are highlighted in light grey and values above 0.99 or below 0.01 indicate strong evidence of a difference in susceptibility between groups and are highlighted in darker grey.

greater susceptivity in the basal ganglia and the hippocampus compared to PCA, and caudate and retrosplenial cortex compared to LPA. Multiple studies reporting differences between controls and tAD have shown increased susceptibilities in the basal ganglia, particularly in the caudate (Acosta-Cabronero et al. 2013; Kim et al. 2017), putamen (Acosta-Cabronero et al. 2013; Du et al. 2018; Cogswell et al. 2021) and the pallidum (Tiepolt et al. 2018; Cogswell et al. 2021), along with the hippocampus (Kim et al. 2017) in both mild and moderate tAD patients. The cingulate gyrus is more controversial with mixed reports supporting higher iron burden within this regions (Kim et al. 2017), while others did not detect any significant differences (Hwang et al. 2016; Ayton et al. 2017). This study highlights the same regions with susceptibility differences compared to the atypical AD variants, which further supports the theory that iron deposition patterns in AD largely depend on the underlying syndromic diagnosis. However, we cannot rule out a potential influence of age since older age has been associated with higher susceptibility in basal ganglia (Lin, Chao, and Wu 2015; Larsen et al. 2020; Cogswell et al. 2021).

The only cognitive profile differences noted between PCA, and LPA were on the Rey-O Complex Figure, VOSP Cubes and Letters, where PCA performed worse than LPA. We were underpowered to detect anything but large effects in the LPA cohort, which could explain why LPA did not perform significantly worse on the BNT and BDAE repetition than PCA, even though the median scores were in the expected direction. Future studies with larger cohorts will be needed to determine whether cognitive performance relates to susceptibility in these patients. The age of onset did not statistically differ between the PCA and LPA, with the PCA cohort having the youngest median onset age, although both PCA and LPA cohorts were younger than the tAD cohort. It is important to note, that PCA showed greater susceptibility in multiple regions when compared to LPA and tAD. One hypothesis that could explain this would be an increase in susceptibility with earlier age of onset in AD, consistent with what we observe with neurodegeneration and tau deposition (Whitwell et al. 2019), though this remains to be explored further.

Strengths of this study include the novelty of using QSM to quantify the magnetic susceptibility of tissue at the voxel-level in the PCA and LPA atypical variants of AD, as no studies have explored QSM in these syndromes. Our study also has some limitations. We had limited statistical power due to the relatively small sample size of the LPA group meaning we may be missing moderate or small effect sizes in our analyses, and we would therefore need a larger LPA cohort to identify smaller differences. All patients were diagnosed by two expert behavioral neurologists, although our battery lacked formal testing of grammar. We compared many regions in our analysis, although our Bayesian methods are prospectively managing the type I error rate (false positive results) and there is no need for further post-hoc corrections. Our disease groups differed by age. While we included age in the models, it is difficult to fully account for the influence of age, as it would be difficult to resolve the effect of age on the disease characteristics of atypical and typical variants of Alzheimer's disease. It is important to highlight that QSM is not a direct measure of brain iron content, but a technique that provides an accurate measurement of the magnetic susceptibility of the tissue and produces a voxel-wise mapping of the mean tissue susceptibility which is its greatest advantage over traditional susceptibility imaging techniques (Wang and Liu 2015; Haacke et al. 2015). We are unable to identify which source of iron contributes to the signal, whether iron is the cause or a consequence of the pathology, or how much it contributes to the pathology. We also cannot account for the effect of myelin's weak diamagnetic signal in white matter (Langkammer et al. 2012). From the literature we know, the effect of myelin in the basal ganglia is minimal (Langkammer et al. 2012) with post-mortem studies establishing a strong correlation between QSM signal and iron content (Sun et al. 2015; Hametner et al. 2018). Additionally, substantia nigra is a major iron storage site, abundant in neuromelanin, which would suggest the dominant signal for QSM in this region would be iron (Haining and Achat-Mendes 2017). Leading to the hypothesis that the contribution of myelin's susceptibility would be minimal, and the dominant signal would remain paramagnetic, originating from iron (Langkammer et al. 2012; Chen et al. 2021), with the overall QSM signal at most being somewhat underestimated (Habib et al. 2012; Betts et al.
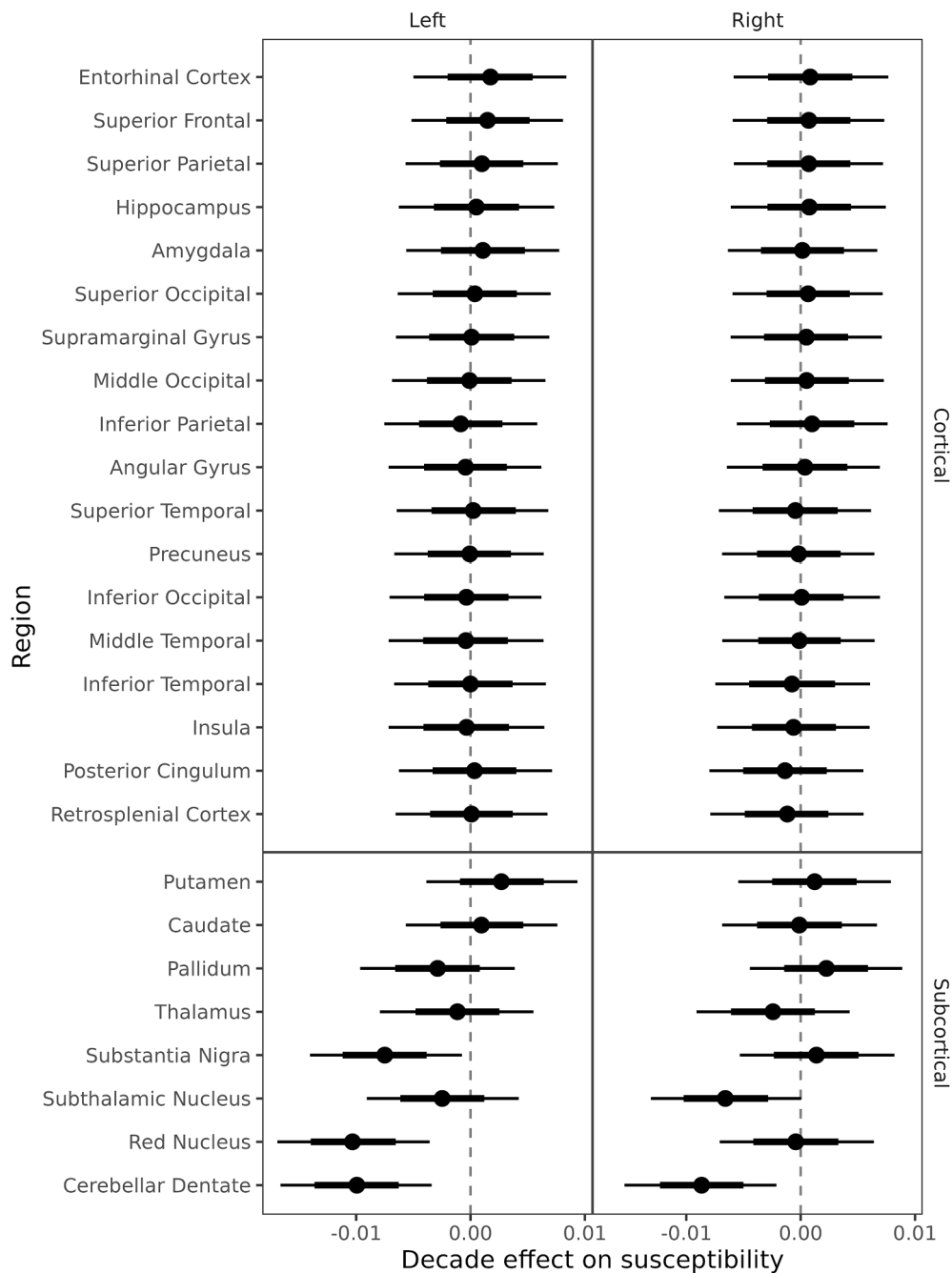
Fig. 4. Forest plots showing the effect of age on regional susceptibility in healthy controls. It is interpreted as follows; when the 80 % posterior interval does not touch zero, we say there is moderate evidence (Pb > 0.90) of difference and when the 98 % posterior interval does not touch zero, we say there is strong evidence (Pb > 0.99) of difference from healthy controls.

2016; Raab et al. (2021)).

5. Conclusion

Our results suggest that iron deposition is a feature of PCA and LPA that can be detected with QSM with iron deposition observed in the occipital, parietal, and temporal regions in PCA, and in the caudate, insula, parietal, and temporal regions for LPA. There is also evidence of increased susceptibility in the atypical AD variants when compared to tAD and heathy controls. These findings contribute to our understanding of brain iron changes in atypical AD and suggest that regional patterns of QSM susceptibility could have some diagnostic utility in AD, although larger studies will be needed to investigate this possibility.

CRediT authorship contribution statement

Neha Atulkumar Singh: Conceptualization, Data curation, Formal analysis, Visualization, Writing – original draft, Writing – review & editing. **Arvin Arani:** Data curation, Formal analysis. **Jonathan Graff-Radford:** Data curation, Formal analysis. **Matthew L. Senjem:** Data curation, Formal analysis. **Peter R. Martin:** Data curation, Formal

Table 4
Posterior probabilities for the effect of age on regional susceptibilities in healthy controls.

		Healthy controls	
	Region	Left	Right
Corticals	Entorhinal Cortex	0.724	0.611
	Superior Frontal	0.697	0.594
	Superior Parietal	0.635	0.600
	Hippocampus	0.571	0.602
	Amygdala	0.645	0.521
	Superior Occipital	0.549	0.591
	Supramarginal Gyrus	0.513	0.567
	Middle Occipital	0.513	0.571
	Inferior Parietal	0.617	0.633
	Angular Gyrus	0.561	0.552
	Superior Temporal	0.532	0.563
	Precuneus	0.509	0.527
	Inferior Occipital	0.550	0.510
	Middle Temporal	0.557	0.518
	Inferior Temporal	0.501	0.608
	Insula	0.546	0.587
	Posterior Cingulum	0.549	0.686
	Retrosplenial Cortex	0.511	0.664
Subcorticals	Putamen	0.826	0.665
	Caudate	0.630	0.517
	Pallidum	0.843	0.782
	Thalamus	0.656	0.799
	Substantia Nigra	0.996	0.682
	Subthalamic Nucleus	0.802	0.989
	Red Nucleus	> 0.999	0.557
	Cerebellar Dentate	> 0.999	0.999

The posterior probabilities of differences in susceptibility between diagnosis groups were calculated based on the region-specific Bayesian models. In this table, any values below 0.10 or above 0.90 indicate moderate evidence of a difference in susceptibility and are highlighted in light grey and values above 0.99 or below 0.01 indicate strong evidence of a difference in susceptibility between groups and are highlighted darker grey.

analysis, Visualization, Writing – original draft, Writing – review & editing. **Mary M. Machulda:** Data curation, Formal analysis. **Christopher G. Schwarz:** Data curation, Formal analysis. **Yunhong Shu:** Data curation, Formal analysis. **Petrice M. Cogswell:** Data curation, Formal analysis. **David S. Knopman:** Data curation, Formal analysis. **Ronald C. Petersen:** Data curation, Formal analysis. **Val J. Lowe:** Data curation, Formal analysis. **Clifford R. Jack:** Data curation, Formal analysis. **Keith A. Josephs:** Conceptualization, Data curation, Formal analysis, Visualization, Writing – original draft, Writing – review & editing. **Jennifer L. Whitwell:** Conceptualization, Data curation, Formal analysis, Visualization, Writing – original draft, Writing – review & editing. All authors revised the text for intellectual content.

Declaration of Competing Interest

The authors declare the following financial interests/personal relationships which may be considered as potential competing interests: Dr. Singh, Dr. Arvin, Dr. Cogswell and Peter Martin have no disclosures to report. Dr. Whitwell, Dr. Machulda, Dr. Schwarz and Dr. Josephs reported receiving research funding from the NIH. Dr. Graff-Radford reported receiving research support from the NIH and he also serves as an editorial board member for Neurology. Matthew Senjem reported holding stock in Gilead Sciences, Inc., Inovio Pharmaceuticals, Medtronic, Oncothyreon, Inc., and PAREXEL International. Dr. Jack reported serving on an independent data monitoring board for Roche, has consulted for and served as a speaker for Eisai, and consulted for Biogen, but he receives no personal compensation from any commercial entity. He receives research support from NIH, the GHR foundation and the Alexander Family Alzheimer's Disease Research Professorship of the Mayo Clinic. Dr. Lowe reported consulting for Bayer Schering Pharma, Piramal Life Sciences, Life Molecular Imaging, Eisai Inc., AVID

Radiopharmaceuticals, and Merck Research and receiving research support from GE Healthcare, Siemens Molecular Imaging, AVID Radiopharmaceuticals and the NIH (NIA, NCI). Dr. Peterson reported serving on scientific advisory boards for Elan Pharmaceuticals and GE Healthcare, he receives royalties from publishing mild cognitive impairment (Oxford University Press, 2003) and receives research support from NIH. Dr. Knopman reported serving on the DSMB of the DIAN-TU study, he is a site PI for clinical trials sponsored by Biogen, Lilly and the University of Southern California and is funded by NIH. Dr. Shu reported being an investor in C3T technologies which have been licensed to GE Healthcare by Mayo Clinic..

Data availability

The data that has been used is confidential.

References

Acosta-Cabronero, J., Williams, G.B., Cardenas-Blanco, A., Arnold, R.J., Lupson, V., Nestor, P.J., 2013. In vivo quantitative susceptibility mapping (QSM) in Alzheimer's disease. PLoS ONE 8, e81093.

Ahmed, S., Irish, M., Loane, C., Baker, I., Husain, M., Thompson, S., Blanco-Duque, C., Mackay, C., Zamboni, G., Foxe, D., Hodges, J.R., Piguet, O., Butler, C., 2018. Association between precuneus volume and autobiographical memory impairment in posterior cortical atrophy: Beyond the visual syndrome. Neuroimage Clin 18, 822–834.

Ayton, S., Wang, Y., Diouf, I., Schneider, J.A., Brockman, J., Morris, M.C., Bush, A.I., 2020. Brain iron is associated with accelerated cognitive decline in people with Alzheimer pathology. Mol. Psychiatry 25, 2932–2941.

Ayton, S., A. Fazlollahi, P. Bourgeat, P. Raniga, A. Ng, Y. Y. Lim, I. Diouf, S. Farquharson, J. Fripp, D. Ames, J. Doecke, P. Desmond, R. Ordidge, C. L. Masters, C. C. Rowe, P. Maruff, V. L. Villemagne, Biomarkers Australian Imaging, Group Lifestyle Research, O. Salvado, and A. I. Bush. 2017. 'Cerebral quantitative susceptibility mapping predicts amyloid-beta-related cognitive decline', Brain, 140: 2112-19.

Ballard, K.J., Savage, S., Leyton, C.E., Vogel, A.P., Hornberger, M., Hodges, J.R., 2014. Logopenic and nonfluent variants of primary progressive aphasia are differentiated by acoustic measures of speech production. PLoS ONE 9, e89864.

Bartzokis, G., Lu, P.H., Tingus, K., Peters, D.G., Amar, C.P., Tishler, T.A., Finn, J.P., Villablanca, P., Altshuler, L.L., Mintz, J., Neely, E., Connor, J.R., 2011. Gender and iron genes may modify associations between brain iron and memory in healthy aging. Neuropsychopharmacology 36, 1375–1384.

Betts, M.J., Acosta-Cabronero, J., Cardenas-Blanco, A., Nestor, P.J., Duzel, E., 2016. High-resolution characterisation of the aging brain using simultaneous quantitative susceptibility mapping (QSM) and R2* measurements at 7T. Neuroimage 138, 43–63.

Botha, H., Duffy, J.R., Whitwell, J.L., Strand, E.A., Machulda, M.M., Schwarz, C.G., Reid, R.I., Spychalla, A.J., Senjem, M.L., Jones, D.T., Lowe, V., Jack, C.R., Josephs, K.A., 2015. Classification and clinicoradiologic features of primary progressive aphasia (PPA) and apraxia of speech. Cortex 69, 220–236.

Chen, Q., Boeve, B.F., Forghanian-Arani, A., Senjem, M.L., Jack Jr., C.R., Przybelski, S.A., Lesnick, T.G., Kremers, W.K., Fields, J.A., Schwarz, C.G., Gunter, J.L., Trzasko, J.D., Graff-Radford, J., Savica, R., Knopman, D.S., Dickson, D.W., Ferman, T.J., Graff-Radford, N., Petersen, R.C., Kantarci, K., 2021. MRI quantitative susceptibility mapping of the substantia nigra as an early biomarker for Lewy body disease. J. Neuroimaging 31, 1020–1107.

Cogswell, P.M., Wiste, H.J., Senjem, M.L., Gunter, J.L., Weigand, S.D., Schwarz, C.G., Arani, A., Therneau, T.M., Lowe, V.J., Knopman, D.S., Botha, H., Graff-Radford, J., Jones, D.T., Kantarci, K., Vemuri, P., Boeve, B.F., Mielke, M.M., Petersen, R.C., Jack Jr., C.R., 2021. Associations of quantitative susceptibility mapping with Alzheimer's disease clinical and imaging markers. Neuroimage 224, 117433.

Crutch, S.J., Lehmann, M., Schott, J.M., Rabinovici, G.D., Rossor, M.N., Fox, N.C., 2012. Posterior cortical atrophy. Lancet Neurol. 11, 170–178.

Crutch, S.J., Schott, J.M., Rabinovici, G.D., Murray, M., Snowden, J.S., van der Flier, W. M., Dickerson, B.C., Vandenberghe, R., Ahmed, S., Bak, T.H., Boeve, B.F., Butler, C., Cappa, S.F., Ceccaldi, M., de Souza, L.C., Dubois, B., Felician, O., Galasko, D., Graff-Radford, J., Graff-Radford, N.R., Hof, P.R., Krolak-Salmon, P., Lehmann, M., Magnin, E., Mendez, M.F., Nestor, P.J., Onyike, C.U., Pelak, V.S., Pijnenburg, Y., Primativo, S., Rossor, M.N., Ryan, N.S., Scheltens, P., Shakespeare, T.J., Suarez Gonzalez, A., Tang-Wai, D.F., Yong, K.X.X., Carrillo, M., Fox, N.C., Association, I.A.

A.D.A., Interest, A.A.S.P., 2017. Consensus classification of posterior cortical atrophy. Alzheimers Dement 13, 870–884.

Dronse, J., Fliessbach, K., Bischof, G.N., von Reutern, B., Faber, J., Hammes, J., Kuhnert, G., Neumaier, B., Onur, O.A., Kukolja, J., van Eimeren, T., Jessen, F., Fink, G.R., Klockgether, T., Drzezga, A., 2017. In vivo Patterns of Tau Pathology, Amyloid-beta Burden, and Neuronal Dysfunction in Clinical Variants of Alzheimer's Disease. J. Alzheimers Dis. 55, 465–471.

Du, L., Zhao, Z., Cui, A., Zhu, Y., Zhang, L., Liu, J., Shi, S., Fu, C., Han, X., Gao, W., Song, T., Xie, L., Wang, L., Sun, S., Guo, R., Ma, G., 2018. Increased Iron Deposition on Brain Quantitative Susceptibility Mapping Correlates with Decreased Cognitive Function in Alzheimer's Disease. ACS Chem. Neurosci. 9, 1849–1857.

Garcia-Azorin, D., Matias-Guiu, J.A., Cabrera-Martin, M.N., Fernandez-Matarrubia, M., Moreno-Ramos, T., Carreras, J.L., Matias-Guiu, J., 2014. Primary progressive aphasia with occipital impairment. J. Neurol. Sci. 347, 387–388.

Gelman, A., Hill, J. (Eds.), 2007. Data Analysis Using Regression and Multilevel/Hierarchical Models. Cambridge University Press.

Goodglass, H., Barresi, B., 2000. Boston Diagnostic Aphasia Examination: Short Form Record Booklet 2000.

Goodrich, B, J Gabry, I Ali, and S Brilleman. 2020. 'Bayesian applied regression modeling via Stan. R package version 2.21.1 '.

Gorno-Tempini, M.L., Dronkers, N.F., Rankin, K.P., Ogar, J.M., Phengrasamy, L., Rosen, H.J., Johnson, J.K., Weiner, M.W., Miller, B.L., 2004. Cognition and anatomy in three variants of primary progressive aphasia. Ann. Neurol. 55, 335–346.

Gorno-Tempini, M.L., Hillis, A.E., Weintraub, S., Kertesz, A., Mendez, M., Cappa, S.F., Ogar, J.M., Rohrer, J.D., Black, S., Boeve, B.F., Manes, F., Dronkers, N.F., Vandenberghe, R., Rascovsky, K., Patterson, K., Miller, B.L., Knopman, D.S., Hodges, J.R., Mesulam, M.M., Grossman, M., 2011. Classification of primary progressive aphasia and its variants. Neurology 76, 1006–1014.

Greenland, S., 2000. Principles of multilevel modelling. Int. J. Epidemiol. 29, 158–167.

Haacke, E.M., Liu, S., Buch, S., Zheng, W., Wu, D., Ye, Y., 2015. Quantitative susceptibility mapping: current status and future directions. Magn. Reson. Imaging 33, 1–25.

Habib, C.A., Liu, M., Bawany, N., Garbern, J., Krumbein, I., Mentzel, H.J., Reichenbach, J., Magnano, C., Zivadinov, R., Haacke, E.M., 2012. Assessing abnormal iron content in the deep gray matter of patients with multiple sclerosis versus healthy controls. AJNR Am. J. Neuroradiol. 33, 252–258.

Haining, R.L., Achat-Mendes, C., 2017. Neuromelanin, one of the most overlooked molecules in modern medicine, is not a spectator. Neural Regen Res 12, 372–435.

Hallgren, B., Sourander, P., 1958. The effect of age on the non-haemin iron in the human brain. J. Neurochem. 3, 41–51.

Hametner, S., Endmayr, V., Deistung, A., Palmrich, P., Prihoda, M., Haimburger, E., Menard, C., Feng, X., Haider, T., Leisser, M., Kock, U., Kaider, A., Hoftberger, R., Robinson, S., Reichenbach, J.R., Lassmann, H., Traxler, H., Trattnig, S., Grabner, G., 2018. The influence of brain iron and myelin on magnetic susceptibility and effective transverse relaxation - A biochemical and histological validation study. Neuroimage 179, 117–133.

Howard, D., and K. Patterson. 1992. *The pyramids and palm trees test: A test of semantic access from words and picture.* (Thames Valley Test Company.).

Hwang, E.J., Kim, H.G., Kim, D., Rhee, H.Y., Ryu, C.W., Liu, T., Wang, Y., Jahng, G.H., 2016. Texture analyses of quantitative susceptibility maps to differentiate Alzheimer's disease from cognitive normal and mild cognitive impairment. Med. Phys. 43, 4718.

Josephs, K.A., Whitwell, J.L., Boeve, B.F., Knopman, D.S., Tang-Wai, D.F., Drubach, D.A., Jack Jr., C.R., Petersen, R.C., 2006. Visual hallucinations in posterior cortical atrophy. Arch. Neurol. 63, 1427–1432.

Josephs, K.A., Pham, N.T.T., Graff-Radford, J., Machulda, M.M., Lowe, V.J., Whitwell, J.L., 2022. Medial Temporal Atrophy in Posterior Cortical Atrophy and Its Relationship to the Cingulate Island Sign. J. Alzheimers Dis. 86 (1), 491–498.

Kertesz, A., 2007. Western Aphasia Battery-Revised. San Antonio, TX, The Psychological Corporation.

Kim, H.G., Park, S., Rhee, H.Y., Lee, K.M., Ryu, C.W., Rhee, S.J., Lee, S.Y., Wang, Y., Jahng, G.H., 2017. Quantitative susceptibility mapping to evaluate the early stage of Alzheimer's disease. Neuroimage Clin 16, 429–438.

Lane, D.J.R., Ayton, S., Bush, A.I., 2018. Iron and Alzheimer's Disease: An Update on Emerging Mechanisms. J. Alzheimers Dis. 64, S379–S395.

Langkammer, C., Schweser, F., Krebs, N., Deistung, A., Goessler, W., Scheurer, E., Sommer, K., Reishofer, G., Yen, K., Fazekas, F., Ropele, S., Reichenbach, J.R., 2012. 'Quantitative susceptibility mapping (QSM) as a means to measure brain iron? A post mortem validation study'. *Neuroimage* 62, 1593–1599.

Lansing, A.E., Ivnik, R.J., Cullum, C.M., Randolph, C., 1999. An empirically derived short form of the Boston naming test. Arch Clin Neuropsychol 14, 481–487.

Larsen, B., Bourque, J., Moore, T.M., Adebimpe, A., Calkins, M.E., Elliott, M.A., Gur, R. C., Gur, R.E., Moberg, P.J., Roalf, D.R., Ruparel, K., Turetsky, B.I., Vandekar, S.N., Wolf, D.H., Shinohara, R.T., Satterthwaite, T.D., 2020. Longitudinal Development of Brain Iron Is Linked to Cognition in Youth. J. Neurosci. 40, 1810–2188.

Lehmann, M., Crutch, S.J., Ridgway, G.R., Ridha, B.H., Barnes, J., Warrington, E.K., Rossor, M.N., Fox, N.C., 2011. Cortical thickness and voxel-based morphometry in posterior cortical atrophy and typical Alzheimer's disease. Neurobiol. Aging 32, 1466–1476.

Li, W., Wu, B., Liu, C., 2011. Quantitative susceptibility mapping of human brain reflects spatial variation in tissue composition. Neuroimage 55, 1645–1656.

Lin, P.Y., Chao, T.C., Wu, M.L., 2015. Quantitative susceptibility mapping of human brain at 3T: a multisite reproducibility study. AJNR Am. J. Neuroradiol. 36, 467–474.

Liu, C., Li, W., Tong, K.A., Yeom, K.W., Kuzminski, S., 2015. Susceptibility-weighted imaging and quantitative susceptibility mapping in the brain. J. Magn. Reson. Imaging 42, 23–41.

Lombardi, J., Mayer, B., Semler, E., Anderl-Straub, S., Uttner, I., Kassubek, J., Diehl-Schmid, J., Danek, A., Levin, J., Fassbender, K., Fliessbach, K., Schneider, A., Huppertz, H.J., Jahn, H., Volk, A., Kornhuber, J., Landwehrmeyer, B., Lauer, M., Prudlo, J., Wiltfang, J., Schroeter, M.L., Ludolph, A., Otto, M., Ftld consortium, 2021. Quantifying progression in primary progressive aphasia with structural neuroimaging. Alzheimers Dement 17, 1595–1609.

Madhavan, A., Whitwell, J.L., Weigand, S.D., Duffy, J.R., Strand, E.A., Machulda, M.M., Tosakulwong, N., Senjem, M.L., Gunter, J.L., Lowe, V.J., Petersen, R.C., Jack Jr., C. R., Josephs, K.A., 2013. FDG PET and MRI in logopenic primary progressive aphasia versus dementia of the Alzheimer's type. PLoS ONE 8, e62471.

McKhann, G.M., Knopman, D.S., Chertkow, H., Hyman, B.T., Jack, C.R., Kawas, C.H., Klunk, W.E., Koroshetz, W.J., Manly, J.J., Mayeux, R., Mohs, R.C., Morris, J.C., Rossor, M.N., Scheltens, P., Carrillo, M.C., Thies, B., Weintraub, S., Phelps, C.H., 2011. The diagnosis of dementia due to Alzheimer's disease: recommendations from the National Institute on Aging-Alzheimer's Association workgroups on diagnostic guidelines for Alzheimer's disease. Alzheimers Dement 7 (3), 263–269.

Nasreddine, Z.S., Phillips, N.A., Bedirian, V., Charbonneau, S., Whitehead, V., Collin, I., Cummings, J.L., Chertkow, H., 2005. The Montreal Cognitive Assessment, MoCA: a brief screening tool for mild cognitive impairment. J. Am. Geriatr. Soc. 53, 695–699.

Osterrieth, P.A., 1944. Le test de copie d'une figure complexe. Archives de psychologie 30, 206–356.

R Core, Team. 2020. 'R: A language and environment for statistical computing.', *R Foundation for Statistical Computing, Vienna, Austria.*

Raab, P., Ropele, S., Bültmann, E., Salcher, R., Lanfermann, H., Wattjes, M.P., 2021. Analysis of deep grey nuclei susceptibility in early childhood: a quantitative susceptibility mapping and R2* study at 3 Tesla. Neuroradiology 64 (5), 1021–1031.

Ramanan, S., Roquet, D., Goldberg, Z.L., Hodges, J.R., Piguet, O., Irish, M., Lambon Ralph, M.A., 2020. Establishing two principal dimensions of cognitive variation in logopenic progressive aphasia. Brain Commun 2, fcaa125.

Ravanfar, P., Loi, S.M., Syeda, W.T., Van Rheenen, T.E., Bush, A.I., Desmond, P., Cropley, V.L., Lane, D.J.R., Opazo, C.M., Moffat, B.A., Velakoulis, D., Pantelis, C., 2021. Systematic review: quantitative susceptibility mapping (QSM) of brain iron profile in neurodegenerative diseases. Front. Neurosci. 15, 618435.

Rohrer, J.D., Caso, F., Mahoney, C., Henry, M., Rosen, H.J., Rabinovici, G., Rossor, M.N., Miller, B., Warren, J.D., Fox, N.C., Ridgway, G.R., Gorno-Tempini, M.L., 2013. Patterns of longitudinal brain atrophy in the logopenic variant of primary progressive aphasia. Brain Lang. 127, 121–126.

Savage, S., Hsieh, S., Leslie, F., Foxe, D., Piguet, O., Hodges, J.R., 2013. Distinguishing subtypes in primary progressive aphasia: application of the Sydney language battery. Dement. Geriatr. Cogn. Disord. 35, 208–218.

Stan Development, Team. 2017. 'Stan Modeling Language Users Guide and Reference Manual, 2.21.0'.

Sun, H., Walsh, A.J., Lebel, R.M., Blevins, G., Catz, I., Lu, J.Q., Johnson, E.S., Emery, D.J., Warren, K.G., Wilman, A.H., 2015. Validation of quantitative susceptibility mapping with Perls' iron staining for subcortical gray matter. Neuroimage 105, 486–492.

Telling, N.D., Everett, J., Collingwood, J.F., Dobson, J., van der Laan, G., Gallagher, J.J., Wang, J., Hitchcock, A.P., 2017. Iron Biochemistry is Correlated with Amyloid Plaque Morphology in an Established Mouse Model of Alzheimer's Disease. Cell Chem Biol 24 (1205–15), e3.

Tetzloff, K.A., Graff-Radford, J., Martin, P.R., Tosakulwong, N., Machulda, M.M., Duffy, J.R., Clark, H.M., Senjem, M.L., Schwarz, C.G., Spychalla, A.J., Drubach, D.A., Jack, C.R., Lowe, V.J., Josephs, K.A., Whitwell, J.L., 2018. Regional Distribution, Asymmetry, and Clinical Correlates of Tau Uptake on [18F]AV-1451 PET in Atypical Alzheimer's Disease. J. Alzheimers Dis. 62, 1713–1724.

Tiepolt, S., Schafer, A., Rullmann, M., Roggenhofer, E., Brain, B.N., Gertz, H.J., Schroeter, M.L., Patt, M., Bazin, P.L., Jochimsen, T.H., Turner, R., Sabri, O., Barthel, H., 2018. Quantitative Susceptibility Mapping of Amyloid-beta Aggregates in Alzheimer's Disease with 7T MR. J. Alzheimers Dis. 64, 393–404.

Tiepolt, S., Rullmann, M., Jochimsen, T.H., Gertz, H.J., Schroeter, M.L., Patt, M., Sabri, O., Barthel, H., 2020. Quantitative susceptibility mapping in beta-Amyloid PET-stratified patients with dementia and healthy controls - A hybrid PET/MRI study. Eur. J. Radiol. 131, 109243.

Tsai, P.H., Teng, E., Liu, C., Mendez, M.F., 2011. Posterior cortical atrophy: evidence for discrete syndromes of early-onset Alzheimer's disease. Am J Alzheimers Dis Other Demen 26, 413–418.

Valdes Hernandez, M.D.C., Reid, S., Mikhael, S., Pernet, C., Neuroimaging, I.A.D., 2018. Do 2-year changes in superior frontal gyrus and global brain atrophy affect cognition? Alzheimers Dement (Amst) 10, 706–716.

Wang, Y., Liu, T., 2015. Quantitative susceptibility mapping (QSM): Decoding MRI data for a tissue magnetic biomarker. Magn. Reson. Med. 73, 82–101.

Warrington, EK, and M James. 1991. *The Visual Object and Space Perception Battery 1991* (Thames Valley Test Company Bury St Edmunds).

Whitwell, J.L., Jack Jr., C.R., Kantarci, K., Weigand, S.D., Boeve, B.F., Knopman, D.S., Drubach, D.A., Tang-Wai, D.F., Petersen, R.C., Josephs, K.A., 2007. Imaging correlates of posterior cortical atrophy. Neurobiol. Aging 28, 1051–1061.

Whitwell, J.L., Martin, P., Graff-Radford, J., Machulda, M.M., Senjem, M.L., Schwarz, C. G., Weigand, S.D., Spychalla, A.J., Drubach, D.A., Jack Jr., C.R., Lowe, V.J., Josephs, K.A., 2019. The role of age on tau PET uptake and gray matter atrophy in atypical Alzheimer's disease. Alzheimers Dement 15, 675–685.

Yamamoto, A., Shin, R.W., Hasegawa, K., Naiki, H., Sato, H., Yoshimasu, F., Kitamoto, T., 2002. Iron (III) induces aggregation of hyperphosphorylated tau and its reduction to iron (II) reverses the aggregation: implications in the formation of neurofibrillary tangles of Alzheimer's disease. J. Neurochem. 82, 1137–1147.